

Spin dynamics in a Curie-switch

A. F. Kravets,^{1,2,*} A. I. Tovstolytkin,¹ Yu. I. Dzhezherya,¹ D. M. Polishchuk,^{1,2} I. M. Kozak,¹ and V. Korenivski²

¹*Institute of Magnetism, National Academy of Sciences of Ukraine, 36 b Vernadsky Blvd., 03142 Kyiv, Ukraine*

²*Nanostructure Physics, Royal Institute of Technology, 10691 Stockholm, Sweden*

(Dated: June 10, 2015)

Ferromagnetic resonance properties of $F_1/f/F_2/AF$ multilayers, where weakly ferromagnetic spacer f is sandwiched between strongly ferromagnetic layers F_1 and F_2 , with F_1 being magnetically soft and F_2 – magnetically hard due to exchange pinning to antiferromagnetic layer AF , are investigated. Spacer-mediated exchange coupling is shown to strongly affect the resonance fields of both F_1 and F_2 layers. Our theoretical calculations as well as measurements show that the key magnetic parameters of the spacer, which govern the ferromagnetic resonance in $F_1/f/F_2/AF$, are the magnetic exchange length (Λ), effective saturation magnetization at $T = 0$ (m_0), and effective Curie temperature (T_C^{eff}). The values of these key parameters are deduced from the experimental data for multilayers with $f = \text{Ni}_x\text{Cu}_{100-x}$, for the key ranges in Ni-concentration ($x = 54 \div 70$ at. %) and spacer thickness ($d = 3 \div 6$ nm). The results obtained provide a deeper insight into thermally-controlled spin precession and switching in magnetic nanostructures, with potential applications in spin-based oscillators and memory devices.

PACS numbers: 76.50.+g, 75.30.Et, 75.70.-i, 85.70.Kh

I. INTRODUCTION

Spin valves, whose central functional part contains two ferromagnetic layers (F_1 , F_2) separated by a nonmagnetic spacer, have been the foundation for a wide range of applications in nanoelectronics and spintronics.^{1–3} Recent studies have demonstrated that incorporation of diluted ferromagnetic layer (f) instead of the nonmagnetic spacer layer may expand the functionality of the spin valves, yielding nanostructures with thermally-controlled magnetic properties, of $F_1/f/F_2$ generic type.^{4–7} In such structures, the exchange coupling between strongly ferromagnetic outer layers F_1 and F_2 depends on whether the temperature is higher or lower than the effective Curie temperature of the spacer (T_C^{eff}). At low temperatures, $T < T_C^{\text{eff}}$, the direct exchange interaction through the spacer in its ferromagnetic state favors the parallel orientation of the magnetic moments M_1 and M_2 of the outer layers, F_1 and F_2 . At high temperatures, $T > T_C^{\text{eff}}$, M_1 and M_2 are exchange decoupled and their orientations can be changed independently by applying a suitable external magnetic field, H . Thus, a variation in temperature and/or field can produce switching between the parallel (P) and antiparallel (AP) mutual orientations of M_1 and M_2 in the system.^{8,9}

The key element in the $F_1/f/F_2$ sandwich described above (the so-called *Curie-switch* or *Curie-valve*) is the weakly ferromagnetic spacer, f , which should have a narrow ferromagnetic-to-paramagnetic transition and have the T_C^{eff} value tunable in fabrication. Diluted ferromagnetic alloys, such as Ni-Cu, is the natural choice for the spacer material, since the Curie temperature of bulk¹⁰ as well as film^{11–14} samples of $\text{Ni}_x\text{Cu}_{100-x}$ alloys depends almost linearly on Ni concentration.

The experiments described in Refs. 8 and 9 confirmed the concept of temperature-controlled P to AP switching in nanostructures $F_1/f/F_2$, in particular containing a

$\text{Ni}_x\text{Cu}_{100-x}$ ($x = 35 \div 72$ at. %) spacer enclosed by an exchange-pinned $\text{Co}_{90}\text{Fe}_{10}$ layer and a free $\text{Ni}_{80}\text{Fe}_{20}$ (Py) layer: $\text{Py}/\text{Ni}_x\text{Cu}_{100-x}/\text{Co}_{90}\text{Fe}_{10}/\text{Mn}_{80}\text{Ir}_{20}$ (hereinafter – $F_1/f/F_2/AF$, AF denoting antiferromagnetic $\text{Mn}_{80}\text{Ir}_{20}$). Since the earlier work primarily aimed at understanding the switching effect itself, little attention was paid to the effect of the spacer-mediated exchange on the ferromagnetic resonance in the structure.

This work investigates the magnetic resonance properties of the Curie-switch, experimentally and theoretically, aiming at understanding the mechanisms involved and obtaining the intrinsic physical parameters governing the spin dynamics in the system.

II. THEORY

Consider an $F_1/f/F_2/AF$ multilayer outlined above, where a weakly ferromagnetic spacer (f) is sandwiched between magnetically soft (F_1) and hard (F_2) layers, with F_2 exchange pinned by an antiferromagnetic layer (AF). The thicknesses of F_1 , F_2 and f are l_1 , l_2 , and d , respectively.

Our calculations of the magnetic resonance fields will assume that F_1 and F_2 are single domain. For small layer thicknesses and strong exchange interaction, in the weak excitation limit typical of ferromagnetic resonance (FMR) experiments, this assumption is well justified.¹⁵ Spacer f with magnetization m provides a relatively weak coupling between the outer ferromagnets, F_1 and F_2 . The analysis aims to determine the effect of this interlayer exchange coupling, variable in strength as a function of temperature, on the FMR.

We use the classical Landau-Lifshitz approach^{16,17} to describe the $F_1/f/F_2/AF$ multilayer and focus on the case where the quasistatic external field H and the alternating field h are in the film plane. Axes Ox and Oy are directed

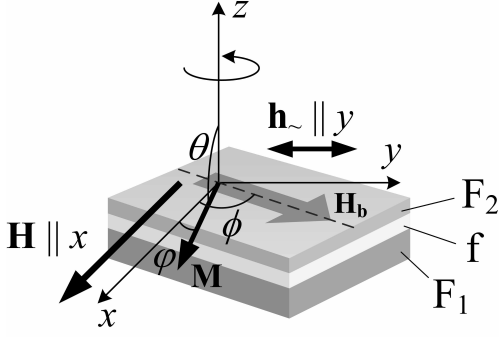


FIG. 1. (Color online) Schematic of $F_1/f/F_2/AF$ multilayer and chosen coordinate system in FMR measurements.

along H and h , respectively (Fig. 1). With Oz perpendicular to the film plane, the magnetization vectors of F_1 and F_2 can be expressed as

$$\mathbf{M}_i = M_i(\sin \theta_i \cos \varphi_i, \sin \theta_i \sin \varphi_i, \cos \theta_i), \quad (1)$$

where $i = 1, 2$; M_i is the saturation magnetization of i -th layer; θ_i and φ_i are the polar and azimuthal angles, respectively.

The exchange bias between F_2 and AF can be modelled using an effective biasing field H_b acting only on magnetization M_2 .¹⁸ It will be shown below that for fully describing the FMR-effects of interest in this work, it is sufficient to consider only two cases, for which the external field H is either parallel or antiparallel to H_b . Correspondingly, the value of H_b can be either positive ($\phi = 0$ in Fig. 1) or negative ($\phi = \pi$) along the biasing axis.

The magnetic energy of the i -th ferromagnetic layer in the above geometrical notations is

$$W_i = S l_i w_i, \quad (2a)$$

$$w_i = 2\pi M_i^2 \cos^2 \theta_i - M_i H_i \cos \varphi_i \sin \theta_i - M_i h \sin \varphi_i \sin \theta_i, \quad (2b)$$

where S is the area of the film surface, w_i is the i -th layer energy density, $H_1 = H$, and $H_2 = H + H_b$. The first terms in Eq. (2b) originates from demagnetizing energy, while the second and third terms describe the energies of the interaction of the layers' magnetizations with the quasi-static H and alternating h external magnetic fields, respectively.

To simplify the equations, let us recall that in the case of a thin film, its high out-of-plane demagnetization fields

prevent the magnetization vector from strongly deviating from the xOy plane. In this case, θ_i can be represented as $\theta_i = \pi/2 + \varepsilon_i$, where $|\varepsilon_i| \ll 1$.

In the small-signal approximation relevant for FMR, the magnetization vectors of F_1 and F_2 are nearly aligned with the Ox axis (the easy axis, also the direction of external field H) and perform only weak oscillations near the ground state under the microwave excitation h . This means that $|\varphi_i| \ll 1$. The limits of validity of this approximation will be discussed in the experimental section below.

In the above small-signal thin-film approximation, the magnetic energy density of the system becomes

$$w_i = -M_i H_i + (4\pi M_i^2 + M_i H_i) \varepsilon_i^2 / 2 + M_i H_i \varphi_i^2 / 2 - M_i h \varphi_i. \quad (3)$$

F_1 and F_2 are exchange coupled through a weakly ferromagnetic spacer f . The case where the spacer is highly magnetically diluted and nominally (in the bulk) is paramagnetic was considered in Ref. 9, with the interlayer exchange mediated via induced proximity ferromagnetism. Here we consider the case where the spacer is diluted such that it is nominally ferromagnetic and can mediate direct exchange between the outer ferromagnetic layers, with the exchange coupling strength being a steep function of temperature near the Curie point of the spacer.

We denote the temperature dependent saturation magnetization of the spacer as m . Assuming again that the magnetization is uniform in the xOy plane, the spacer energy density can be written as

$$w = \frac{\alpha m^2}{2} \left[\left(\frac{\partial \theta}{\partial z} \right)^2 + \sin^2 \theta \left(\frac{\partial \varphi}{\partial z} \right)^2 \right] - \frac{\mathbf{m} \mathbf{H}_m}{2} - H m \cos \varphi \sin \theta - h m \sin \theta \sin \varphi, \quad (4)$$

where α is the constant of exchange interaction, θ and φ are polar and azimuthal angles, respectively, of the spacer magnetic moment \mathbf{m} , \mathbf{H}_m is the magnetostatic field in the system.

The value of the magnetostatic field can be easily derived from Maxwell's equation: $\text{div} \mathbf{B} = \text{div}(\mathbf{H}_m + 4\pi \mathbf{m}) = 0$. Since both the magnetization and therefore magnetostatic field depend only on one special variable, z , the magnetostatic field becomes: $\mathbf{H}_m = -4\pi m \cos \theta \mathbf{e}_z = -4\pi m \cos \theta \mathbf{e}_z$, where \mathbf{e}_z is the unit vector along the z axis.

Taking into account Eq. (4), the Landau-Lifshitz equations in the angular form become

$$\frac{\partial^2 \theta}{\partial \xi^2} = -\frac{d^2}{\Lambda^2} \left[\sin \theta \cos \theta + \sin \theta \frac{\partial \varphi}{\partial \tau} + \frac{H}{4\pi m} \cos \theta \cos \varphi + \frac{h}{4\pi m} \cos \theta \sin \varphi \right], \quad (5a)$$

$$\frac{\partial}{\partial \xi} \left(\sin^2 \theta \frac{\partial \varphi}{\partial \xi} \right) = \frac{d^2}{\Lambda^2} \left[\sin \theta \frac{\partial \varphi}{\partial \tau} + \frac{H}{4\pi m} \sin \theta \sin \varphi - \frac{h}{4\pi m} \sin \theta \cos \varphi \right]. \quad (5b)$$

The new dimensionless variables, normalized to the characteristic length and time in the problem, introduced in Eqs. (5a) and (5b) are $\xi = z/d$ and $\tau = 4\pi t \gamma m$, where t is the time and γ is the gyromagnetic ratio. $\Lambda = \sqrt{\alpha/4\pi}$ is the magnetic exchange length.¹⁹

If the spacer thickness d is much smaller than the magnetic exchange length Λ ($d \ll \Lambda$), the right side in Eqs. (5a) and (5b) becomes a small correction, which in the first approximation can be neglected.

As a result, only the exchange terms survive:

$$\frac{\partial^2 \theta}{\partial \xi^2} = 0, \quad (6a)$$

$$\frac{\partial}{\partial \xi} \left(\sin^2 \theta \frac{\partial \varphi}{\partial \xi} \right) = 0. \quad (6b)$$

The solution, which satisfies the requirement of continuity of the polar and azimuthal components at the interfaces between the layers, has the form:

$$\begin{aligned} \varphi(z) &= \varphi_2 + (\varphi_1 - \varphi_2)z/d, \\ \varepsilon(z) &= \varepsilon_2 + (\varepsilon_1 - \varepsilon_2)z/d, \\ 0 &\leq z \leq d. \end{aligned} \quad (7)$$

The resulting magnetic energy of the spacer is

$$W = SJ [(\varphi_1 - \varphi_2)^2 + (\varepsilon_1 - \varepsilon_2)^2] / 2, \quad (8)$$

where $J = \alpha m^2 / d = 4\pi \Lambda^2 m^2 / d$.

To determine the resonance conditions for the layered system under consideration, we express the Lagrange function in terms of the angle:

$$L = \sum_{i=1}^2 \left(-Sl_i \frac{M_i}{\gamma} \varepsilon_i \frac{\partial \varphi_i}{\partial t} - W_i \right) + J [(\varphi_1 - \varphi_2)^2 + (\varepsilon_1 - \varepsilon_2)^2] / 2. \quad (9)$$

The variational equations following from Eq. (9) are equivalent to the Landau-Lifshitz equations:

$$\begin{pmatrix} iH_\omega & H + h_1 & 0 & -h_1 \\ 4\pi M_1 + H + h_1 & -iH_\omega & -h_1 & 0 \\ 0 & -h_2 & iH_\omega & H + H_b + h_2 \\ -h_2 & 0 & 4\pi M_2 + H + H_b + h_2 & -iH_\omega \end{pmatrix} \times \begin{pmatrix} \varepsilon_1 \\ \varphi_1 \\ \varepsilon_2 \\ \varphi_2 \end{pmatrix} = \begin{pmatrix} h \\ 0 \\ h \\ 0 \end{pmatrix} \quad (10)$$

where $h_i = J/M_i l_i = \alpha m^2 / d M_i l_i = 4\pi \Lambda^2 m^2 / d M_i l_i$. Here, $H_\omega = \omega / \gamma$, $\omega = 2\pi f$, γ is the gyromagnetic ratio, h_i is the characteristic field of exchange interaction between the layers.

The characteristic fields of the resonance modes of

the collective spin dynamics in the system are found by equating the determinant of matrix (10) to zero. This results in two branches in the functional form of $H_\omega(H)$.

The first resonance branch, corresponding to the resonance field of F_1 , has the form:

$$\begin{aligned} H_\omega^2 &= (H_{r1} + h_1)(4\pi M_1 + H_{r1} + h_1) - h_1 h_2 \left[1 - \frac{(2\pi M_1 + H_{r1})(2\pi M_2 + H_{r1})}{2\pi H_{r1}(M_2 - M_1)} \right] \\ &\quad - h_1 h_2 \frac{H_b}{H_{r1}} \frac{4\pi [\pi(M_2 + M_1) + H_{r1}](M_2 - M_1) - (2\pi M_1 + H_{r1})(2\pi M_2 + H_{r1})}{[2\pi(M_2 - M_1)]^2}, \end{aligned} \quad (11)$$

where H_{r1} is the external field producing FMR in F_1 [see Fig. 2 (a)]. Only terms of order not higher than quadratic in k_i were kept in Eq. (11).

The value of H_{r1} depends on whether the external magnetic field is parallel ($\uparrow\uparrow$) or antiparallel ($\uparrow\downarrow$) to the exchange bias field H_b . It is easy to show that the difference in the resonance fields, $\Delta H_{r1} = H_{r1}^{\uparrow\downarrow} - H_{r1}^{\uparrow\uparrow}$, has the form:

$$\Delta H_{r1} = H_{r1}^{\uparrow\downarrow} - H_{r1}^{\uparrow\uparrow} = h_1 h_2 \frac{H_b}{H_{r1}^0} \frac{4\pi [\pi(M_2 + M_1) + H_{r1}^0] (M_2 - M_1) - (2\pi M_1 + H_{r1}^0)(2\pi M_2 + H_{r1}^0)}{(2\pi M_1 + H_{r1}^0) [2\pi(M_2 - M_1)]^2}, \quad (12)$$

where $H_{r1}^0 = (H_{r1}^{\uparrow\downarrow} + H_{r1}^{\uparrow\uparrow})/2 = \sqrt{(2\pi M_1)^2 + H_\omega^2} - 2\pi M_1 - h_1$.

It follows from Eq. (12) that ΔH_{r1} is proportional to a product of $h_1 h_2$. This means that ΔH_{r1} sharply changes in the vicinity of the Curie point of the spacer as a result of the sharp increase in m at the para-to-ferromagnetic transition (see Eq. (10)). Expectedly, ΔH_{r1} goes to zero as T increases above the Curie point of the spacer. In this high- T limit, there is no coupling between F_1 and F_2 , and Eq. (11) describes the resonance field of the decoupled soft outer ferromagnet F_1 .

To find the resonance fields for F_2 , we keep only terms of the order not higher than linear in h_i . The results for $H_{r2}^{\uparrow\downarrow}$ and $H_{r2}^{\uparrow\uparrow}$ are

$$\begin{aligned} H_{r2}^{\uparrow\uparrow} &= \sqrt{(2\pi M_2)^2 + H_\omega^2} - 2\pi M_2 - h_2 - H_b, \\ H_{r2}^{\uparrow\downarrow} &= \sqrt{(2\pi M_2)^2 + H_\omega^2} - 2\pi M_2 - h_2 + H_b. \end{aligned} \quad (13)$$

Again, sharp changes in $H_{r2}^{\uparrow\uparrow}$ and $H_{r2}^{\uparrow\downarrow}$ are expected in the vicinity of the Curie point of the spacer. At high temperatures where $h_2 \rightarrow 0$, the difference between $H_{r2}^{\uparrow\downarrow}$ and $H_{r2}^{\uparrow\uparrow}$ naturally becomes $2H_b$.

It follows from Eq. (13) that for sufficiently high values of M_2 and h_2 , the $H_{r2}^{\uparrow\uparrow}$ branch can fall into negative fields, where it cannot be observed experimentally.

III. EXPERIMENT

A. Samples and measurements

The experiments were carried out on two sets of multilayered samples, in which either the spacer thickness, d , or its composition, x , were varied. The first set was Py(10 nm)/Ni₅₄Cu₄₆(d)/Co₉₀Fe₁₀(5 nm)/Mn₈₀Ir₂₀(12 nm) (hereinafter – F₁/Ni₅₄Cu₄₆(d)/F₂/AF) with the spacer thicknesses $d = 3, 4.5, \text{ and } 6$ nm. The second set was Py(10 nm)/Ni _{x} Cu_{100- x} (6 nm)/Co₉₀Fe₁₀(5 nm)/Mn₈₀Ir₂₀(12 nm) (hereinafter – F₁/Ni _{x} Cu_{100- x} (6 nm)/F₂/AF), with $x = 54, 62 \text{ and } 70$ at.%. The multilayers were deposited at room temperature on thermally oxidized silicon substrates using magnetron sputtering in an AJA Orion 8-target system. The exchange pinning between the ferromagnetic Co₉₀Fe₁₀ and antiferromagnetic Mn₈₀Ir₂₀ was set in during deposition of the multilayers using an in-plane magnetic field $H_{\text{dep}} \approx 1$ kOe. Other fabrication details are similar to those described in Refs. 8 and 9.

In addition to the multilayers, single-layer Py (10 nm) and Co₉₀Fe₁₀ (5 nm) films were prepared under identical technological conditions. FMR measurements on the single-layer films were carried out to extract the magnetizations of Py and Co₉₀Fe₁₀ layers and use them for

subsequent multilayer-FMR modelling and characterization [e.g., using Eqs. (12) and (13)].

The FMR measurements were performed using an X-band ELEXSYS E500 spectrometer equipped with an automatic goniometer. The operating frequency was $f = 9.44$ GHz. FMR spectra for various in-plane dc-field angles were studied in the temperature range of 120 to 400 K.

B. Results and discussion

1. Measured FMR spectra

Fig. 2 (a) shows two typical FMR spectra for a F₁/f/F₂/AF multilayer, for which the external magnetic field is parallel (solid line) or antiparallel (red dashed line) to the exchange bias field H_b ($T = 300$ K). The resonance signals from both F_1 and F_2 layers are clearly visible and are separated in field. As expected [see Eqs. (12) and (13)], the resonance conditions for both layers depend on the mutual orientation of H and H_b [Fig. 2(b)]. Consistent with the predicted behavior of Eq. (13), the $H_{r2}^{\uparrow\uparrow}$ branch for F_2 extrapolates into negative fields [see Fig. 2(b)]. In the remainder of the paper we therefore discuss and in-depth analyze only the $H_{r2}^{\uparrow\downarrow}$ resonance branch as regards the dynamics of the pinned F_2 layer.

To understand the details of how the interlayer exchange coupling affects the spin dynamics of the free layer (F_1), the angular dependence of H_{r1} was studied at various temperatures for various spacer thicknesses. The typical data shown in Fig. 3 indicate that the position of the resonance peak is angle-dependent and this angular asymmetry becomes stronger as the temperature is lowered. At the same time, the H_{r1} vs ϕ dependence becomes more pronounced as the spacer thickness decreases. For all the cases shown in Figs. 2 (b) and 3, each $H_{r1}(\phi)$ data set is well fitted using a model characteristic of a thin film with unidirectional anisotropy (solid lines in Fig. 2 (b) and Fig. 3).

A more detailed analysis shows that there is an additional small contribution from uniaxial anisotropy. The extracted uniaxial anisotropy field (~ 4 Oe) is weakly dependent on temperature and spacer composition. This contribution potentially originates from some ordered configuration at NiCu/Py interface formed during the multilayer deposition in a magnetic field H_{dep} (used for exchange pinning F_2).

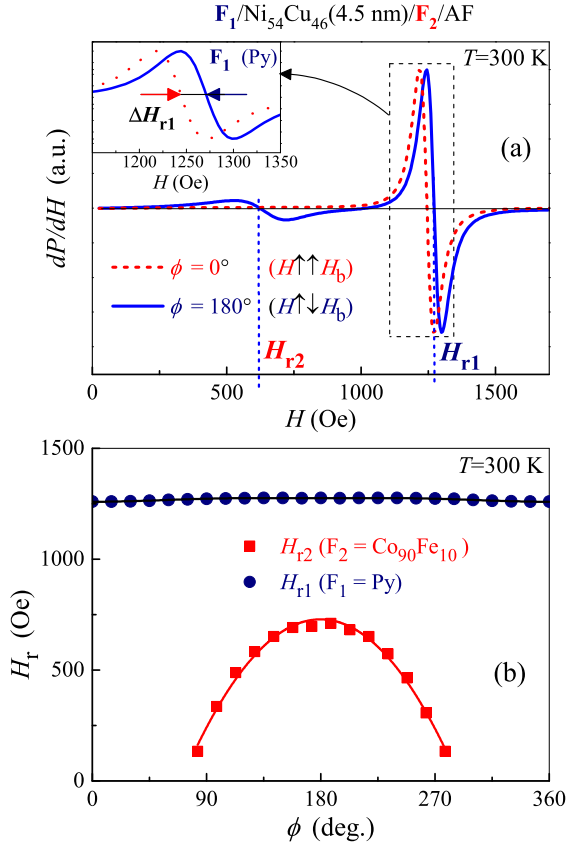


FIG. 2. (Color online) (a) FMR spectra for $F_1/\text{Ni}_{54}\text{Cu}_{46}(4.5 \text{ nm})/F_2/\text{AF}$ for parallel (solid line) and antiparallel (red dashed line) orientations of the external magnetic field H with respect to the exchange biasing field H_b . The upper inset shows an enlarged view of the signal from F_1 . (b) The dependence of the resonance fields of F_1 and F_2 on the angle ϕ between H and H_b extracted from data sets such as those illustrated in (a).

2. FMR modelling procedure

Expressions (12) and (13) were used for calculating the temperature dependence of the resonance field asymmetry $\Delta H_{r1} = H_{r1}^{\uparrow\downarrow} - H_{r1}^{\uparrow\uparrow}$ for F_1 (Py), and of the resonance field $H_{r2}^{\uparrow\downarrow}$ for F_2 ($\text{Co}_{90}\text{Fe}_{10}$). These expressions contain the values of the saturation magnetization M_1 and M_2 for the Py and $\text{Co}_{90}\text{Fe}_{10}$ layers, respectively, which are temperature dependent. The $M_1(T)$ and $M_2(T)$ dependences, used in the data analysis to follow, are shown in Fig. 4 and were obtained from the FMR data taken on single-layer Py (10 nm) and $\text{Co}_{90}\text{Fe}_{10}$ (5 nm) films prepared under the same conditions as the multilayers. The Kittel's formulas for isotropic thin films^{20,21} were used to calculate the $M_1(T)$ and $M_2(T)$ shown.

The key quantity determining the behavior of ΔH_{r1} and $H_{r1}^{\uparrow\downarrow}$, is the spacer magnetization m , averaged over the layer thickness [see Eq. (10)]. The spacer is ferromagnetic below the Curie point and nominally paramagnetic

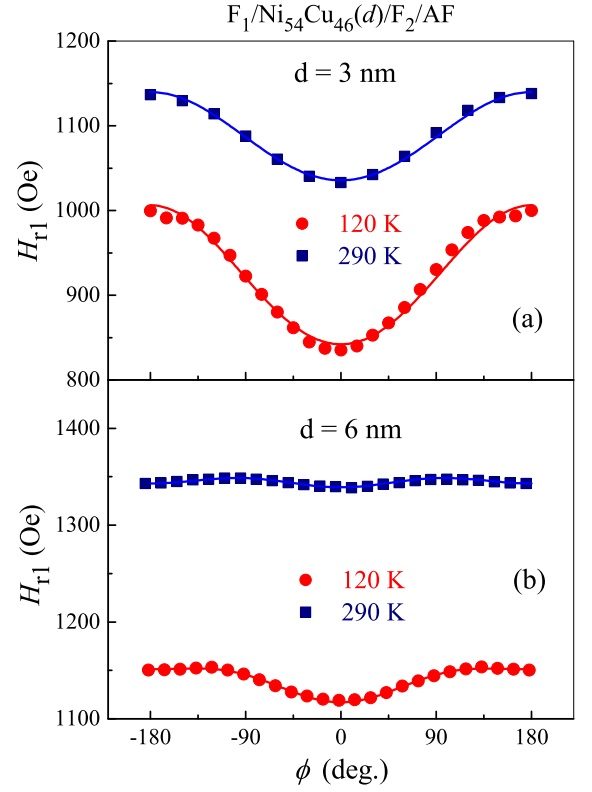


FIG. 3. (Color online) Angular dependences of the resonance fields of the soft layer (F_1) in $F_1/\text{Ni}_{54}\text{Cu}_{46}(d)/F_2/\text{AF}$ with the spacer thickness $d = 3 \text{ nm}$ (a) and 6 nm (b).

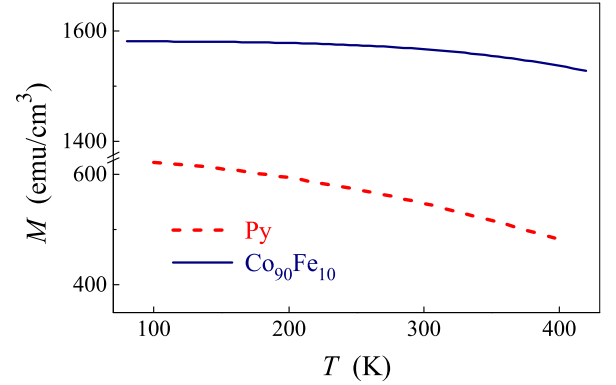


FIG. 4. (Color online) Temperature dependences of the magnetizations of Py and $\text{Co}_{90}\text{Fe}_{10}$ layers obtained from the FMR data on the respective single-layered films.

above it. It has previously been shown, however, that the proximity effect at the interface with a strong ferromagnet induces noticeable magnetization in a paramagnetic or weakly ferromagnetic metal and may give rise to an increase in its Curie point.^{9,22,23} The proximity length is an order of magnitude greater than the atomic spacing and for the case where the spacer thickness d is of

the order of a few nanometers, the induced magnetization penetrates through the spacer thickness.^{8,9} For this reason, to account for the proximity effect in our calculations, it was assumed that (i) there is an additional field H_{prox} which acts on the spacer magnetization m and (ii) for the spacer sandwiched between strong ferromagnets F_1 and F_2 , the Curie point T_C^{eff} differs from that in the bulk.

The $m(T, H_{\text{prox}})$ dependence due to the proximity effect was modelled using the mean-field approximation,^{15,24} where the magnetization is described by the Brillouin function:

$$\frac{m}{m_0} = B_j(m) = \xi_1 \cosh \left[\xi_1 \left(\zeta_1 \frac{m}{T} + \zeta_2 \frac{H_{\text{prox}}}{T} \right) \right] - \xi_2 \cosh \left[\xi_2 \left(\zeta_1 \frac{m}{T} + \zeta_2 \frac{H_{\text{prox}}}{T} \right) \right];$$

$$\xi_1 = \frac{2j+1}{2j}; \xi_2 = \frac{1}{2j}; \zeta_1 = \frac{3j}{j+1} \frac{T_C^{\text{eff}}}{m_0}; \zeta_2 = \nu m_0; \quad (14)$$

where j is the total angular momentum per $\text{Ni}_x\text{Cu}_{100-x}$ formula unit, m_0 is the saturation magnetization at $T = 0$ K, H_{prox} is the effective field reflecting the proximity effect at the interfaces with the strong ferromagnets F_1 and F_2 , and T_C^{eff} is the effective Curie temperature. Coefficient ν equals $\mu/(\rho N_A)$, where μ and ρ are the molar mass and density of $\text{Ni}_x\text{Cu}_{100-x}$, respectively, N_A is the Avogadro constant, and k_B is the Boltzmann constant.^{15,24}

The coefficient ν for our $\text{Ni}_x\text{Cu}_{100-x}$ alloy was estimated to be near $8.2 \times 10^{-8} \text{ cm}^3 \text{ K erg}^{-1}$ for x in the vicinity of 60 at.%. The initial values of j and m_0 were chosen based on the data calculated in Ref. 8 for bulk $\text{Ni}_x\text{Cu}_{100-x}$, and the value of j was kept fixed throughout the analysis. Since the magnetization and Curie temperature of the $\text{Ni}_x\text{Cu}_{100-x}$ spacer are expected to differ from those in the bulk, specifically due to the proximity effect, m_0 was chosen as one of the variable parameters in fitting the experimental data.

The proximity effect is expected to be most pronounced in the vicinity of T_C^{eff} . The *ab-initio* calculations of this effect for $F_1/\text{Ni}_x\text{Cu}_{100-x}(x, d)/F_2/\text{AF}$ at $T \sim T_C^{\text{eff}}$ were detailed in Ref. 9. Based on a comparison of the values for the average magnetic moment $\langle m \rangle$ obtained in Ref. 9 and the $m_{\text{calc}}(T)$ obtained using Eq. 14, it was found that m_{calc} at $T \sim T_C^{\text{eff}}$ is approximately equal to $\langle m \rangle$ for $H_{\text{prox}} \approx 100$ kOe. This value of H_{prox} was kept fixed in all subsequent calculations.

Another important quantity affecting the spin dynamics in the system is the exchange bias field H_b . Based on the magnetometry measurements on $F_1/\text{Ni}_x\text{Cu}_{100-x}(x, d)/F_2/\text{AF}$ reported in Ref. 8, H_b was obtained for a range of x and d values (for 300 K). These and the additional data reported in Ref. 9 make it possible to conclude that for our samples with $x > 52$, H_b is only weakly temperature dependent. The calculation therefore assumed $H_b(T) = \text{const}$. The specific fixed j

and H_b values used in the calculations, among other parameters and variables, are presented in Table I.

Summarizing, the variable parameters used to fit the theoretical $\Delta H_{r1}(T)$ and $H_{r2}^{\uparrow\downarrow}(T)$ to the experimental data were the effective Curie temperature (T_C^{eff}) and saturation magnetization at $T = 0$ (m_0) of the $\text{Ni}_x\text{Cu}_{100-x}$ spacer, as well as the characteristic magnetic exchange length (Λ). It will be shown below that for the case under study, the resulting values of Λ are about two times greater than the spacer thickness d . This is within the limits of the approximation $d \ll \Lambda$ used in the analysis.

3. FMR data analysis

Figs. 5 (a) and (b) show the temperature dependences of $H_{r1}^{\uparrow\downarrow} - H_{r1}^{\uparrow\uparrow}$ and $H_{r2}^{\uparrow\downarrow}$ for $F_1/\text{Ni}_{54}\text{Cu}_{46}(d)/F_2/\text{AF}$ samples obtained from the measured FMR spectra as well as the respective theoretical fits using the above analysis. A good agreement between the experiment and theory is obtained for realistic values of the fitting parameters.

The temperature dependence of the spacer magnetization m/m_0 obtained from fitting the resonance fields is shown in Fig. 5 (c) for different values of the spacer thickness. The proximity of the strongly ferromagnetic layers F_1 and F_2 has essentially no effect on the low-temperature magnetization of the spacer but is the dominant factor determining its effective Curie point T_C^{eff} . The changes in T_C^{eff} strongly depend on the spacer thickness: the smaller the d and, therefore, the stronger the proximity effect of the interfaces, the higher the T_C^{eff} .

Fig. 6 (a, b) shows the measured resonance fields $H_{r1}^{\uparrow\downarrow} - H_{r1}^{\uparrow\uparrow}$ and $H_{r2}^{\uparrow\downarrow}$ as a function of temperature for $F_1/\text{Ni}_x\text{Cu}_{100-x}(6 \text{ nm})/F_2/\text{AF}$ with different Ni-concentration in the spacer, fitted to theory using Eqs. (12) and (13). The agreement is good, including the case of the highest Ni-concentration with non-monotonous temperature dependence of the resonance field asymmetry (70 at.% Ni in Fig. 6 (a)).

The dependence of the spacer magnetization on temperature extracted from fitting the data in Figs. 6 (a, b) is shown in Fig. 6 (c) for different Ni-concentration of the spacer. It is clear in this case that the proximity of the strongly ferromagnetic outer layers affects both the low-temperature magnetization m_0 and the effective Curie point T_C^{eff} of the spacer – the greater the x , the higher the m_0 and T_C^{eff} .

Having performed the data analysis, it is now informative to discuss the accuracy of the theoretical assumption made in Section 2 in describing the spin dynamics in an $F_1/f/F_2/\text{AF}$ spin-thermionic system. One key assumption was that the magnetization vectors of the F_1 and F_2 layers are parallel to the external field H and perform only weak oscillation under the influence of the alternating field component h . This assumption is strictly correct for the case where H is parallel to H_b , but the opposite antiparallel case ($H \uparrow\downarrow H_b$) must be considered with care.

TABLE I. Magnetic parameters of $F_1/Ni_xCu_{100-x}(x, d)/F_2/AF$ multilayers.

x (at.% Ni)	d (nm)	j^a	H_b (Oe) ^b	T_C^{eff} (K)	m_0 (emu/cm ³)	Λ (nm)
0.54	3.0	0.19	180	450	120	11±2
0.54	4.5	0.19	240	320	120	11±2
0.54	6.0	0.19	300	250	120	11±2
0.62	6.0	0.21	280	350	140	12±2
0.70	6.0	0.23	210	550	150	13±2

^a Values calculated from data of Ref. 9 under assumption that Lande g -factor equals 2.

^b Values obtained from magnetic hysteresis loops at room temperature of Ref. 8.

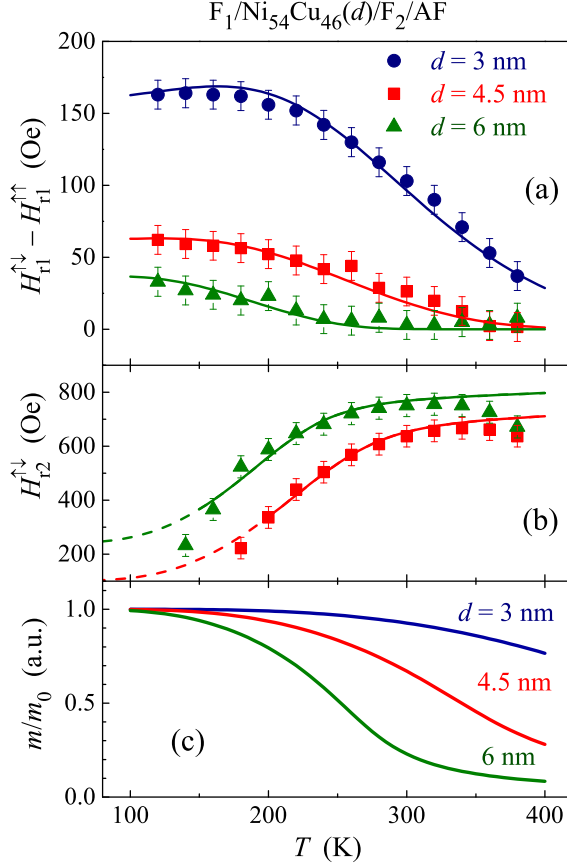


FIG. 5. (Color online) Temperature dependences of $H_{r1}^{\downarrow} - H_{r1}^{\uparrow}$ (a) and H_{r2}^{\downarrow} (b) for $F_1/Ni_{54}Cu_{46}(d)/F_2/AF$ samples for three spacer thicknesses (symbols). Bold solid lines show theoretical $H_{r1}^{\downarrow} - H_{r1}^{\uparrow}$ and H_{r2}^{\downarrow} vs T dependences fitted to the measured data using Eqs. (12) and (13), respectively. (c) Temperature dependence of the normalized spacer magnetization m/m_0 obtained using the above fitting of the resonance fields.

The values of H_b for $F_1/Ni_xCu_{100-x}(x, d)/F_2/AF$ multilayers are listed in Table I. As follows from the $M - H$ data presented in Refs. 8 and 9, the magnetization of the $F_1/f/F_2/AF$ multilayer fully saturates when the applied reversing field H^{\downarrow} exceeds $(1.2 \div 1.5)$ times H_b . Thus, the above assumption should be valid when both resonance fields, H_{r1}^{\downarrow} and H_{r2}^{\downarrow} , are higher than $(1.2 \div$

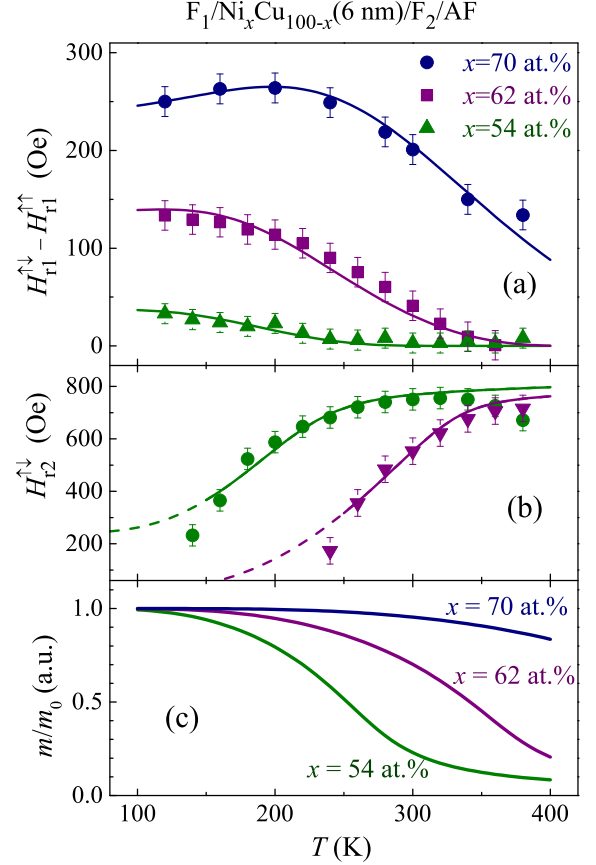


FIG. 6. (Color online) Temperature dependences of $H_{r1}^{\downarrow} - H_{r1}^{\uparrow}$ (a) and H_{r2}^{\downarrow} (b) for $F_1/Ni_xCu_{100-x}(6 \text{ nm})/F_2/AF$ samples for three Ni concentrations (symbols). Bold solid lines show theoretical $H_{r1}^{\downarrow} - H_{r1}^{\uparrow}$ and H_{r2}^{\downarrow} vs T dependences fitted to the measured data using Eqs. (12) and (13), respectively. (c) Temperature dependences of the normalized spacer magnetization m/m_0 obtained using the above fitting of the resonance fields.

$1.5)H_b$. For the samples under study, H_{r1}^{\downarrow} is greater than 900 Oe, so the first condition, $H_{r1}^{\downarrow} > (1.2 \div 1.5)H_b$, is well satisfied. The data in Figs. 5 and 6 indicate that the second condition, $H_{r2}^{\downarrow} > (1.2 \div 1.5)H_b$, is also well satisfied for temperatures above ~ 180 K.

The developed approach, combining theory and ex-

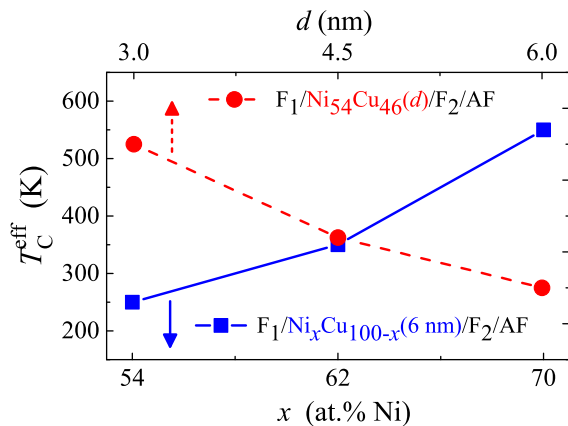


FIG. 7. (Color online) Dependence of the effective Curie point T_C^{eff} of the spacer $\text{Ni}_x\text{Cu}_{100-x}$ on its thickness d (at fixed composition $x = 54$ at.% Ni) and Ni content x (at fixed thickness $d = 6$ nm).

periment, makes it possible to extract and analyze the thickness and composition dependence of the characteristic parameters of the spacer, which are summarized in Table I.

Fig. 7 presents the model-extracted dependence of the effective Curie point T_C^{eff} of the spacer on its thickness d and Ni content x . We conclude that small variations in both d and x result in significant variations in T_C^{eff} . We also note that the values of the Curie temperature of $\text{Ni}_x\text{Cu}_{100-x}$ sandwiched between strong ferromagnets are much greater than the corresponding values in the bulk form of this diluted magnetic alloy – ($T_C^{\text{bulk}} \approx 120$ K and 300 K for $x = 54$ and 70 at.% Ni, respectively)¹⁰.

IV. CONCLUSION

Ferromagnetic resonance properties of $F_1/f/F_2/\text{AF}$ multilayers, where spacer f has a low Curie point compared to strongly ferromagnetic F_1 and F_2 , have been analyzed theoretically and investigated experimentally. The spacer-mediated exchange coupling is shown to strongly affect the resonance fields of both F_1 and F_2 layers. It is found that the key magnetic parameters of the spacer which govern the magnetic resonance in the system are the magnetic exchange length (Λ), the effective saturation magnetization at $T = 0$ (m_0), and the effective Curie temperature (T_C^{eff}) of the spacer.

By theoretically fitting the measured FMR data, the values of Λ , m_0 , and T_C^{eff} are obtained for the technologically significant ranges in Ni-concentration ($x = 54 \div 70$ at.% Ni) and thickness ($d = 3 \div 6$ nm). The values thus obtained are entirely different from the corresponding quantities in the bulk. The developed approach to spin dynamics in the system enables such detailed quantitative characterization that is otherwise difficult or impossible obtain in terms of direct measurements due to the built-in strong proximity effect.

The inferred magnetism in the key element of the structure – the spacer, acting as an interlayer exchange-spring – shows a great sensitivity and thereby high tunability of its properties versus the degree of magnetic dilution, geometry, and temperature. These results should be useful for designing high-speed nanodevices based on spin-thermionic control.

ACKNOWLEDGMENTS

Support from the Swedish Stiftelse Olle Engkvist Buggmästare, Swedish Research Council (VR grant 2014-4548), the Science and Technology Center in Ukraine (project P646), and the National Academy of Sciences of Ukraine (projects 0115U003536 and 0115U00974) are gratefully acknowledged.

* anatolii@kth.se; Correspondence author

¹ B. Dieny, V. S. Speriosu, S. S. P. Parkin, B. A. Gurney, D.

R. Wilhoit, and D. Mauri, Phys. Rev. B **43**, 1297 (1991).

² *Nanomagnetism and Spintronics* edited by T. Shinjo (Elsevier, Amsterdam, 2009).

³ A. Hirohata and K. Takahashi, J. Phys. D: Appl. Phys. **47**, 193001 (2014).

⁴ S. Andersson and V. Korenivski, IEEE Trans. Magn. **46**, 2140 (2010).

⁵ S. Andersson and V. Korenivski, J. Appl. Phys. **107**, 09D711 (2010).

⁶ A. M. Kadigrobov, S. Andersson, D. Radić, R. I. Shekhter, M. Jonson, and V. Korenivski, J. Appl. Phys. **107**, 123706 (2010).

⁷ A. M. Kadigrobov, S. Andersson, Hee Chul Park, D. Radić, R. I. Shekhter, M. Jonson, and V. Korenivski, J. Appl. Phys. **111**, 044315 (2012).

⁸ A. F. Kravets, A. N. Timoshevskii, B. Z. Yanchitsky, M. A. Bergmann, J. Buhler, S. Andersson, and V. Korenivski, Phys. Rev. B **86**, 214413 (2012).

⁹ A. F. Kravets, Yu. I. Dzhezherya, A. I. Tovstolytkin, I. M. Kozak, A. Gryshchuk, Yu. O. Savina, V. A. Pashchenko, S. L. Gnatchenko, B. Koop, and V. Korenivski, Phys. Rev. B **90**, 104427 (2014).

¹⁰ D. J. Chakrabarti, D. E. Laughlin, S. W. Chen, and Y. A. Chang, in *Phase Diagrams of Binary Copper Alloys* edited by P. Subramanian, D. Chakrabarti, and D. Laughlin (ASM International, Materials Park, OH, 1994), p. 276.

- ¹¹ A. P. Thakoor and K. L. Chopra, *J. Appl. Phys.* **48**, 3850 (1977).
- ¹² I. Bakonyi, E. Tóth-Kádár, J. Tóth, T. Becsei, T. Tarnóczy, and P. Kamasa, *J. Phys.: Condens. Matter* **11**, 963 (1999).
- ¹³ A. Rusanov, R. Boogaard, M. Hesselberth, H. Sellier, and J. Aarts, *Physica C* **369**, 300 (2002).
- ¹⁴ A. F. Kravets, A. N. Timoshevskii, B. Z. Yanchitsky, O. Yu. Salyuk, S. O. Yablonovskii, S. Andersson, and V. Korenivski, *J. Magn. Magn. Mater.* **324**, 2131 (2012).
- ¹⁵ A. Aharoni, *Introduction to the Theory of Ferromagnetism* (Oxford University Press, Oxford, 1996).
- ¹⁶ L. D. Landau and E. M. Lifshitz, in *The Collection of Works* edited by L. D. Landau (Nauka, Moscow, 1969) [in Russian], Vol. 1, p. 128.
- ¹⁷ C. Serpico, I. D. Mayergoyz, and G. Bertotti, *J. Appl. Phys.* **93**, 6909 (2003).
- ¹⁸ J. Nogues, J. Sort, V. Langlais, V. Skumryev, S. Surinach, J. S. Muñoz, and M. D. Baro, *Phys. Rep.* **422**, 65 (2005).
- ¹⁹ Gavin S. Abo, Yang-Ki Hong, Jihoon Park, Jaejin Lee, Woncheol Lee, and Byoung-Chul Choi, *IEEE Trans. Magn.* **49**, 4937 (2013).
- ²⁰ Ch. Kittel, *Phys. Rev.* **73**, 155 (1948).
- ²¹ A. G. Gurevich and G. A. Melkov, *Magnetization Oscillations and Waves* (CRC Press, Boca Raton, FL, 1996).
- ²² N. Garcia and A. Hernando, *J. Magn. Magn. Mater.* **99**, L12 (1991).
- ²³ I. Navarro, M. Ortuno, and A. Hernando, *Phys. Rev. B* **53**, 11656 (1996).
- ²⁴ S. Chikazumi, *Physics of Ferromagnetism* (Oxford University Press, New York, 2005).